Advanced Energy Materials

ADVANCED ENERGY MATERIALS
www.advenergymat.de

RESEARCH ARTICLE

Linearly Bonded Organoselenide-Sulfide Hybrid Compound Cathode Materials for High-Capacity and Shuttling-Suppressed Lithium-Organochalcogenide Batteries

Xingkai Ma | Huan Li | Junchuan Liang | Yaoda Wang | Xinmei Song | Zuoao Wu | Huaizhu Wang | Jingyi Wang | Tianchen Yu | Lina Qin | Zuoxiu Tie | Zhong Jin

State Key Laboratory of Coordination Chemistry, MOE Key Laboratory of Mesoscopic Chemistry, MOE Key Laboratory of High Performance Polymer Materials and Technology, Jiangsu Key Laboratory of Green Energy Catalysis and Intelligent Chemical Engineering, Suzhou Key Laboratory of Green Intelligent Manufacturing of New Energy Materials and Devices, Tianchang New Materials and Energy Technologies Research Center, Institute of Green Chemistry and Engineering, School of Chemistry and Chemical Engineering, Nanjing University, Nanjing, Jiangsu, P. R. China

Correspondence: Zhong Jin (zhongjin@nju.edu.cn)

Received: 4 March 2026 | **Revised:** 28 May 2026 | **Accepted:** 8 June 2026

Keywords: cathode | electrochemistry | lithium–sulfur battery

ABSTRACT

Lithium-organochalcogenide batteries have the merits of high energy density, eco-friendliness, and low costs, but facing issues like rapid capacity fading and poor rate capability. Herein, we propose the design and synthesis of an organoselenide-sulfide hybrid compound by reacting tetramethyl thiuram disulfide with molten selenium disulfide (SeS_2). The organoselenide-sulfide hybrid compound possesses a chain-like structure, high chalcogen (S and Se) atom ratios, and enhanced conductivity, capable of serving as a high-capacity and long-cycling cathode material for lithium-organochalcogenide batteries. The 1D linear molecular structure formed through synergistic selenium–sulfur bonding enabled significant enhancement of electrochemical performance via dual mechanisms involving chemical adsorption and electrochemical conversion. Moreover, an array of electrochemical tests and mechanistic analyses verified that this configuration can effectively suppress the shuttle effect during battery cycling and simultaneously enhance material structural stability. The organoselenide-sulfide hybrid compound cathode exhibited a heightened specific capacity (816.8 mAh g^{-1} at 1.0 A g^{-1}) and an improved capacity retention (with a decay of 0.06% per cycle). These dual advantages provide fresh insights into advancing lithium–organochalcogenide battery technology and offer a promising pathway toward their practical implementation.

1 | Introduction

In the realm of energy storage, lithium–chalcogenide batteries have emerged as a subject of intense scientific and industrial interest, owing to their considerable theoretical energy density and affordability [1–10]. When compared to traditional lithium-ion batteries, lithium–sulfur (Li–S) batteries offer a substantially higher theoretical energy density. Nevertheless, the commercial realization of Li–S batteries confronts an array of formidable challenges. One of the most pronounced issues pertains to rapid

Xingkai Ma and Huan Li contributed equally to this work.

capacity fading and limited cycling life, primarily attributed to the intrinsic instability, inherently low ionic conductivity, and shuttling effect of sulfur-based cathode materials [11–13]. In response to these impediments, a multitude of research efforts have been channelled toward addressing the issues. These include applying a nanoporous host matrix or a separator coating layer, which confines the polysulfides to the positive electrode side [14–23]. Additionally, the use of functional additives in the electrolytes has also been considered [24–26]. While these measures can partially alleviate the shuttle effect, they do not eliminate the root cause – the generation and dissolution of polysulfides. Within this backdrop, structurally designable organosulfide cathode materials have attracted considerable attention as cathode materials [27–30]. However, the presence of long sulfur chains in these structures still results in low conductivity, limiting their rate performance. Notably, selenium (Se), a congener of sulfur in the chalcogen group, exhibits an electronic conductivity of $\sim 1 \times 10^{-5}$ S cm^{-1}, which is approximately 25 orders of magnitude higher than that of S (5×10^{-30} S cm^{-1}) [31] – despite its lower theoretical specific capacity (675 mAh g^{-1} vs. 1675 mAh g^{-1} for sulfur). This intriguing property facilitates improved electrode kinetics and utilization of cathode materials. Selenium hybridization offers a dual advantage, concurrently enhancing the electrical conductivity of sulfides while also promoting their stability through chemical adsorption and electrochemical conversion mechanisms [32–36]. However, designing and engineering organoselenide-sulfide compounds as advanced cathode materials for rechargeable lithium–chalcogenide batteries are still largely unexplored.

Herein, we present the design and synthesis of a chain-like organoselenide-sulfide hybrid cathode material, specifically tetramethyl thiuram polyselenosulfide (TMTSeS), by incorporating tetramethyl thiuram disulfide (TMTD) into molten SeS_2. The introduction of selenium represents a pivotal advancement, as it significantly augments the electrical conductivity of organosulfides, while concurrently enhancing stability through chemical adsorption and electrochemical conversion mechanisms. The effectiveness of the TMTSeS cathode material was clearly verified in a series of rigorous electrochemical tests and comprehensive mechanism analyses. These analyses affirmed the remarkable performance of the TMTSeS cathode material in lithium-chalcogenide batteries, characterized by an impressive specific capacity of 816.8 mAh g^{-1} at the current density of 1.0 A g^{-1} and an enhanced cycling stability (with a mere 0.06% capacity decay per cycle). These results underscore the immense potential of organoselenide-sulfide hybrid cathode materials in lithium–chalcogenide batteries toward high-energy-density, low-cost, and sustainable secondary batteries.

2 | Results and Discussion

The TMTSeS cathode material was synthesized by adding TMTD into molten SeS_2 under specific heating conditions, as shown in Figure 1a. For further comparison, tetramethyl thiuram polysulfide (TMTS) and tetramethyl thiuram polyselenide (TMTSe) cathode materials were also prepared as control samples by a similar method, except that the SeS_2 precursor was replaced by elemental S or Se precursor, respectively. The TMTSeS product underwent characterizations using scanning electron microscopy (SEM), and energy-dispersive X-ray spectroscopy (EDX) analyses to determine its elemental compositions. The SEM images, presented in Figure 1b and Figure S1a, exhibit a close-up view of the TMTSeS and TMTD materials, respectively. The presence of key elements in TMTSeS was confirmed through the corresponding EDX analyses in Figure 1c–e, offering insights into the presence of Se and S elements within the material. In the EDX mapping diagrams, the Se and S elements are evenly distributed in TMTSeS, confirming the successful introduction of Se. In contrast, no Se distribution and lower S content are observed in the EDX mappings of TMTD (Figure S1b–d). As shown in Table S1, the elemental analysis results demonstrate that TMTSeS contains high contents of S and Se, which contribute to a high density of lithium storage sites and correspond to a theoretical specific capacity of approximately 1023 mAh g^{-1}. The schematic mechanism diagram of the charge-discharge processes of TMTSeS cathode is illustrated in Figure 1g. At the beginning of the discharge process, chain-like TMTSeS initially turned into Li_2R ($R = (CH_3)_2NCS_2$) and $Li_2(SeS_2)_x$ species. For the Li_2R species, the nitrogen center provided an extra pair of electrons, serving as a Lewis base site to stabilize the anion structure. $Li_2(SeS_2)_x$, featuring both Se and S atoms in the chain structure, was a linear lithium polychalcogenide compound and was insoluble in the electrolyte. Subsequently, $Li_2(SeS_2)_x$ underwent further discharge, producing insoluble Li_2SeS_2, and then Li_2Se and Li_2S. This process benefited from the alternating presence of the more metallic Se within the chain structure, enhancing the conductivity of the cathode and providing abundant energy storage sites. Additionally, it avoided the formation of soluble polysulfides or polyselenides, thereby preventing the shuttle effect and improving cycling stability. As a sharp contrast, the TMTS and TMTSe control samples contained continuous long sulfur or selenium chains in their structures, leading to the generation of soluble polysulfides or polyselenides upon discharge (Figure S2). These long-chain species can readily dissolve into the electrolyte, thus triggering the shuttle effect of TMTS and TMTSe cathodes.

The TMTSeS material was comprehensively analyzed by various characterization techniques, providing essential insights into its structural, chemical, and elemental properties (Figure 2). The structural changes caused by the incorporation of SeS_2 into the TMTD chain were highlighted by the XRD analyses (Figure 2a). The XRD pattern of TMTSeS preserves the characteristic diffraction peaks of TMTD and SeS_2, and exhibits some new diffraction peaks, indicating the successful combination of TMTD and SeS_2. The Fourier-transform infrared (FTIR) spectra provide more information about the molecular compositions and bonding interactions within the TMTSeS material (Figure 2b). The comparison between TMTSeS and TMTD allows the discernment of any new functional groups or chemical changes originated from the interaction between TMTD and SeS_2. Compared to TMTD, the C—S bond signal (1150–1210 cm^{-1}) in TMTSeS is still present and the peak signal of 590 cm^{-1} is strengthened, indicating the presence of S—Se bonds [37]. The chemical bond features in TMTSeS are also presented in the deconvoluted X-ray photoelectron spectroscopy (XPS) analyses at S 2p, Se 3d, and N 1s levels (Figure 2c,d and Figure S3), further verifying the structural constitution of TMTSeS. The high-resolution XPS spectrum of TMTSeS at S 2p level reveals four pairs of deconvoluted peaks at 166.5, 162.7, 161.2, and 159.2 eV, corresponding to S—Se, S—S, C—S, and C═S bonds, respectively (Figure 2c) [38]. In comparison, the high-resolution

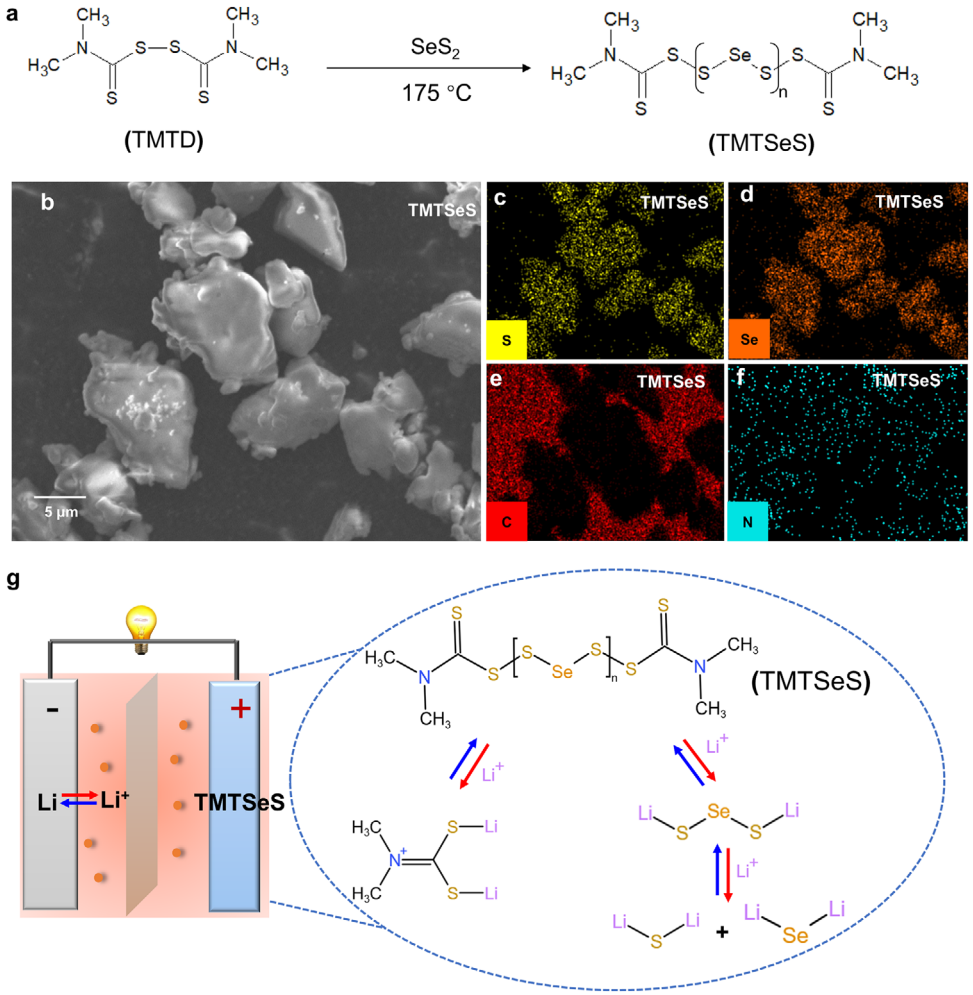

FIGURE 1 | Synthesis, characterizations, and redox mechanism of Organoselenide-Sulfide Hybrid Compound Cathode Material. (a) Schematic illustration of the synthesis process of TMTSeS cathode material. (b) SEM image and (c–f) corresponding EDX analyses of TMTSeS cathode material. (g) Schematic mechanism diagram of the charge-discharge processes of TMTSeS cathode.

XPS spectrum of TMTD at S 2p level exhibits only three pairs of peaks at 162.7, 161.2, and 160.1 eV, with no 166.5 eV peak associated with S—Se bonds (Figure 2c) [38]. The high-resolution XPS spectrum at Se 3d level of TMTSeS (Figure 2d) shows distinct signal peaks, whereas no Se signals are detected for TMTD [39]. In the high-resolution XPS spectra at N 1s level (Figure S3), the deconvoluted peaks at 397.8 and 399.0 eV remain consistent before and after the reaction, corresponding to sp^2-hybridized nitrogen species with lone electron pairs either non-participating or participating in conjugation, respectively, indicating their local chemical environment remains largely unaffected. However, the signal attributed to nitrogen species embedded within the sp^2 carbon framework exhibits a significant shift from 399.8 to 401.2 eV due to the strong electron-withdrawing effect of the Se/S atoms [40]. These results comprehensively verify the successful incorporation of Se into TMTSeS through chemical bonding. In addition, thermogravimetric (TG) analysis of TMTSeS (Figure S4) shows no detectable unreacted SeS_2 residue, further supporting the complete chemical incorporation of Se into TMTSeS.

The electrochemical properties and kinetic performances of TMTSeS cathode were studied by comparing the test results with other samples (Figure 3). The cyclic voltammetry (CV) curves of the TMTSeS, TMTS, TMTSe, and TMTD cathodes at the same scan rate (0.5 mV s^{-1}) show different characteristics of redox peaks (Figure 3a). For TMTSeS cathodes, three reduction peaks (2.30, 2.15, and 2.00 V) and two oxidation peaks (2.28 and 2.41 V) are observed at different potentials, indicating specific lithiation and de-lithiation processes. The CV curve of the TMTS cathode is close to that of conventional lithium–sulfur batteries, indicating that it has a long sulfur chain structure. The CV curve of the TMTSe cathode also shows three reduction peaks, but the corresponding potentials are close to each other (2.10, 2.05, and 1.95 V), which are related to the presence of Se—Se bonds. The peak intensities of the TMTSeS cathode are much higher than those of the TMTS and TMTSe cathodes, indicating that it has the highest electrochemical reactivity among them. The polarization potential of the TMTSeS cathode (0.41 V) is significantly lower than that of the TMTS cathode (0.55 V), but slightly higher than that of the TMTSe cathode (0.39 V), which indicates that the introduction of Se improves its electrochemical kinetics. In contrast, the CV curve of the TMTD cathode only has a pair of redox peaks, corresponding to the binding of S atoms with Li^+ (Figure S2c), and its polarization potential is about 0.7 V. Furthermore, the electrochemical impedance spectroscopy (EIS) analyses could also explain the contribution of Se introduction

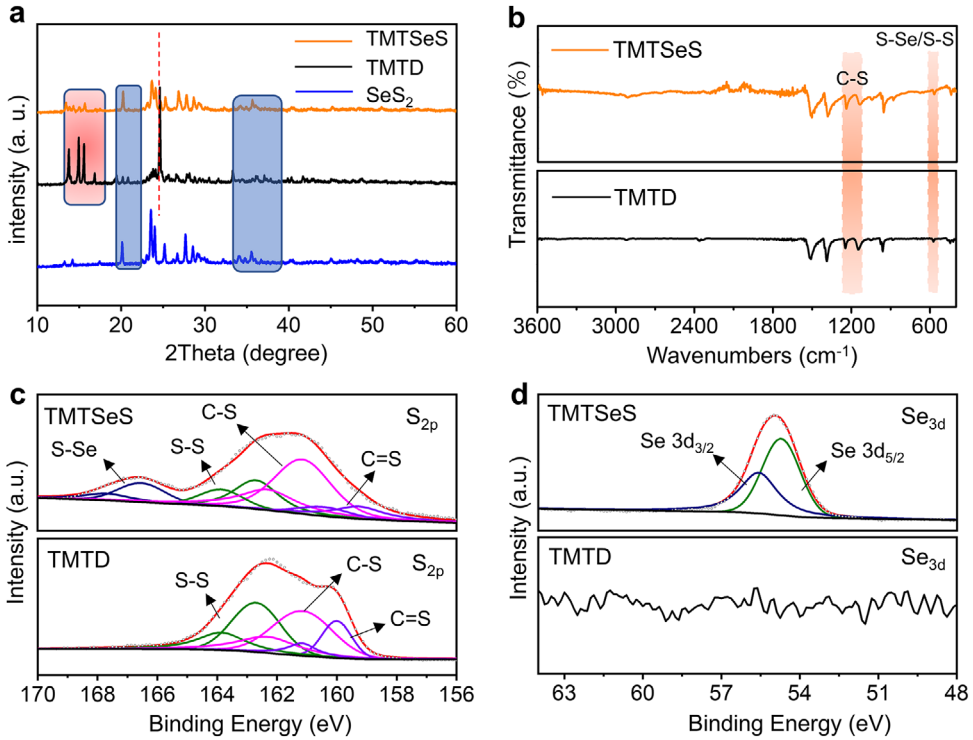

FIGURE 2 | (a) XRD profiles of TMTSeS, TMTD, and SeS_2. (b) FTIR spectra of TMTSeS and TMTD. (c, d) XPS spectra at (c) S 2p and (d) Se 3d levels of TMTSeS and TMTD, respectively.

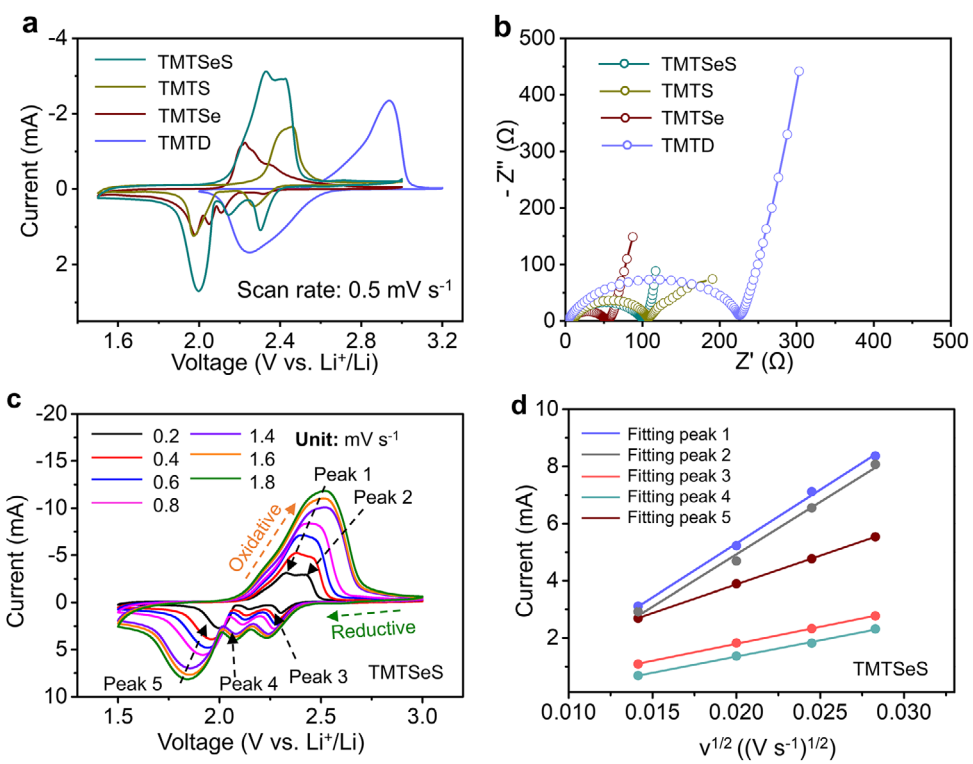

FIGURE 3 | (a) CV curves of TMTSeS, TMTS, TMTSe, and TMTD cathodes at a scan rate of 0.5 mV s^{-1}. (b) EIS analyses of TMTSeS, TMTS, TMTSe, and TMTD cathodes. (c) CV curves and (d) corresponding peak current fitting curves of TMTSeS cathode at various scan rates between 0.2 and 1.8 mV s^{-1}.

on the cathode kinetics (Figure 3b). The TMTSeS, TMTS, and TMTSe cathodes exhibit the charge transfer impedances of 95, 99, and 50 Ω, respectively, which are related to the conductivity enhancement through the introduction of Se. In contrast, the charge transfer impedance of the TMTD cathode is ~225 Ω, which is much higher than the above three cathodes, indicating that its kinetic performance is relatively poor. The electrochemical dynamics of the TMTSeS cathode were investigated by sweeping CV at different scan rates, showing higher response currents as increasing sweeping rates (Figure 3c). A fitted straight line is obtained by correlating the peak current of the cyclic voltammetry curve with the square root of the scan rate at various scan rates (Figure 3d). The diffusion coefficient of lithium-ion (Li^+) in the battery can be estimated according to the Randles-Sevcik formula [41]:

$$I_p = 2.65 \times 10^5 n^{1.5} S D_{Li^+}{}^{0.5} C v^{0.5} \quad (1)$$

where Ip is the peak current (A mg^{-1}), n is the charge transfer number, S is the area of the electrode (cm^2), D_{Li+} is the diffusion coefficient of Li^+ (cm^2 s^{-1}), and C is the amount of Li^+ in the electrolyte concentration in (mol cm^{-3}), and ν is the scan rate (V s^{-1}). Since the influencing factors of the slope of the fitting line are all constant except for D_{Li+}, the slope is only related to the diffusion coefficient of Li^+. Comparing the slopes of the corresponding peak fitted straight lines of TMTSeS (Figure 3d) with those of TMTS, TMTSe, TMTD, and the physically mixed TMTD/Se sample (Figures S5 and S6), it can be found that the slope of TMTSeS is higher, indicating a higher Li^+ diffusion coefficient and thus improved electrochemical kinetics of the TMTSeS cathode. The calculated apparent Li^+ diffusion coefficients are summarized in Tables S2 and S3. Notably, although the physically mixed TMTD/Se sample contains conductive Se species, its Li^+ diffusion kinetics still remain inferior to those of TMTSeS, suggesting that the kinetic enhancement is not solely derived from elemental Se itself, but is closely related to the S–Se chemical bonding configuration. Similarly, the electrical conductivity measurements (Figure S7) also support this conclusion.

The battery performance of the TMTSeS cathode material was evaluated through a series of electrochemical measurements (Figure 4). The TMTSeS cathode demonstrated stable capacities during consecutive charging/discharging operations for 100 cycles at 0.5 A g^{-1}, delivering an initial capacity of 778.0 mAh g^{-1} with a capacity retention of 93.3% (726.2 mAh g^{-1}), suggesting its highly reversible lithiation/delithiation capability (Figure 4a). The broad temperature tolerance of TMTSeS material was further demonstrated by cycling at variable temperatures between 0°C and 90°C at 1.0 A g^{-1} (Figure 4b). At a low temperature of 0°C, the TMTSeS cathode could still cycle normally, and the specific capacity is about 530 mAh g^{-1}. This indicates that TMTSeS has good low-temperature transport capability, attributing to the introduction of Se atoms. With the temperature rising to 60°C and 90°C, the specific capacity of TMTSeS cathode rises to 864.8 and 1021.9 mAh g^{-1}, respectively, suggesting that it has good stability at high temperature. This wide temperature tolerance can be attributed to the introduction of Se atoms, which enhance both the electronic conductivity and structural stability of the cathode. Figure 4c exhibits the rate capabilities of TMTSeS, TMTS, and TMTSe cathodes at various current densities, ranging from 0.2 to 4.0 A g^{-1}. When the current density reaches 4.0 A g^{-1}, the specific capacities of these three materials are 449.3, 230.4, and 87.5 mAh g^{-1}, respectively. The TMTSeS cathode also shows distinguishable voltage plateaus even at a high rate of 4.0 A g^{-1} (Figure 4d), which is indicative of a diffusion-dominated Li-ion storage process rather than a simple capacitive-controlled process. The rate capability measurements offer more insights into the ability of TMTSeS cathode to deliver power at different discharge rates, showcasing its responsiveness to varying power demands. For comparison, the rate performance of the TMTD precursor was also tested under the same conditions (Figure S8). When the current density reaches 4.0 A g^{-1}, the specific capacity of the TMTD cathode is almost negligible, indicating that its rate performance is inferior to that of the TMTSeS cathode.

To further evaluate the long-term cycling performance of TMTSeS cathode material, Li||TMTSeS pouch batteries were assembled and comprehensively tested. As shown in Figure 4e, the soft-packed Li||TMTSeS battery with a high areal TMTSeS loading of 9.3 mg cm^{-2} and a low electrolyte-to-sulfur (E/S) ratio of 3 μL mg^{-1} sustains a specific capacity of ~800 mAh g^{-1} at 0.5 A g^{-1}, retaining ~540 mAh g^{-1} after 100 cycles. In addition, the soft-packed Li||TMTSeS battery delivered a gravimetric energy density of 204.69 Wh kg^{-1}, with the key parameters and electrochemical performances summarized in Table S4. Moreover, the soft-packed Li||TMTSeS can readily power up a panel of red light-emitting diodes (LEDs) and maintain stable brightness under repeated bending (Figure 4f). These results demonstrate good cycling stability and flexibility of the TMTSeS cathode material. Furthermore, during long-term cycling, the TMTSeS cathode delivered an initial capacity of 816.8 mAh g^{-1} at 1.0 A g^{-1}, with a decay of 0.06% per cycle during 600 cycles (Figure 4g). Oppositely, the TMTS and TMTSe cathodes delivered only initial capacities of 554.0 and 449.5 mAh g^{-1} and decreased to 243.3 and 136.8 mAh g^{-1}, corresponding to a higher capacity decay rate of 0.21% and 0.32% per cycle, respectively, during 400 cycles at 1.0 A g^{-1}. For comparison, the long-cycle performance of the TMTD monomer was tested at the same current density (Figure S8). The initial capacity of TMTD cathode was only about 200 mAh g^{-1}, and remained only 87.9 $mAhg^{-1}$ after 200 cycles. These tests confirm the durability and expected lifespan of the TMTSeS cathode during long-term cycles.

To delve into the underlying mechanism governing the charge-discharge processes of the TMTSeS cathode, the Li||TMTSeS batteries were disassembled after long-term cycling, and the retrieved electrode underwent ex situ analyses involving XPS, ultraviolet-visible (UV–vis) absorption spectroscopy, and in situ Raman spectroscopy (Figure 5). These characterization techniques were employed across various cutoff voltages, with the objective of elucidating the Li^+ storage mechanism of TMTSeS and ascertaining the extent of polysulfide formation. The high-resolution XPS spectra at S 2p and Se 3d levels of TMTSeS cathode are illustrated in Figure 5a,b, respectively. At a cutoff voltage of 2.20 V, a pair of deconvoluted peaks appeared at 160.5 eV in the S 2p spectra, corresponding to the S—Li bond, indicating the onset of the lithium storage process in the TMTSeS cathode [36, 42]. As the discharge continued to 1.60 V, the intensity of these peaks increased significantly, representing a further lithiation process, while the deconvoluted peaks at 164.5 eV, corresponding to S—Se and related bonds, decreased noticeably. Upon charging to 2.70 V,

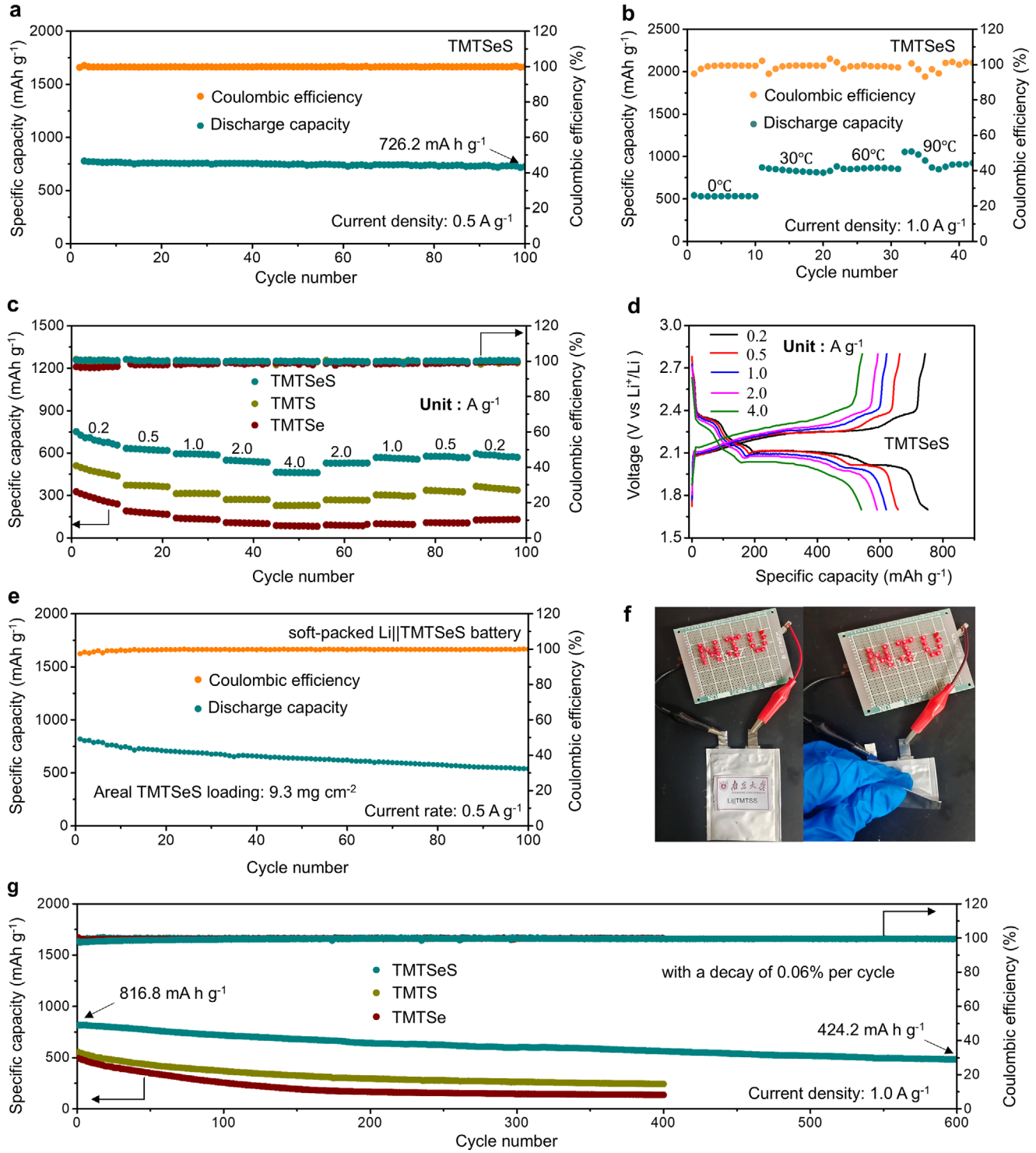

FIGURE 4 | (a) Cycling stability of TMTSeS cathode at a current density of 0.5 A g^{-1}. (b) Cycling stability of TMTSeS cathode at different temperatures. (c) Rate capabilities of TMTSeS, TMTS, and TMTSe cathodes at various current densities from 0.2 to 4.0 A g^{-1}. (d) Galvanostatic discharge/charge profiles of TMTSeS cathode at various current densities from 0.2 to 4.0 A g^{-1}. (e) Cycling performance and coulombic efficiency of soft-packed Li||TMTSeS battery tested at 0.5 A g^{-1}. (f) A patterned LED panel steadily powered by a soft-packed Li||TMTSeS battery. (g) Long-term cycling performances of TMTSeS, TMTS, and TMTSe cathodes at a current density of 1.0 A g^{-1}.

the S—Li signal peak disappeared, and the S—Se related peaks reached maximum intensity, demonstrating a reversible lithium storage process. In the Se 3d XPS spectra, upon discharging to 2.20 V, the intensity of the Se—S peak decreased noticeably, reflecting the cleavage of the S—Se—S bonds in preparation for lithiation. When the TMTSeS cathode was fully discharged to 1.60 V, a deconvoluted peak corresponding to the formation of the Li—Se bond appeared at 54.1 eV, indicating the completion of lithiation. Upon charging to 2.70 V, the Li—Se peak disappeared, while the Se–S peak reached its maximum intensity, indicating

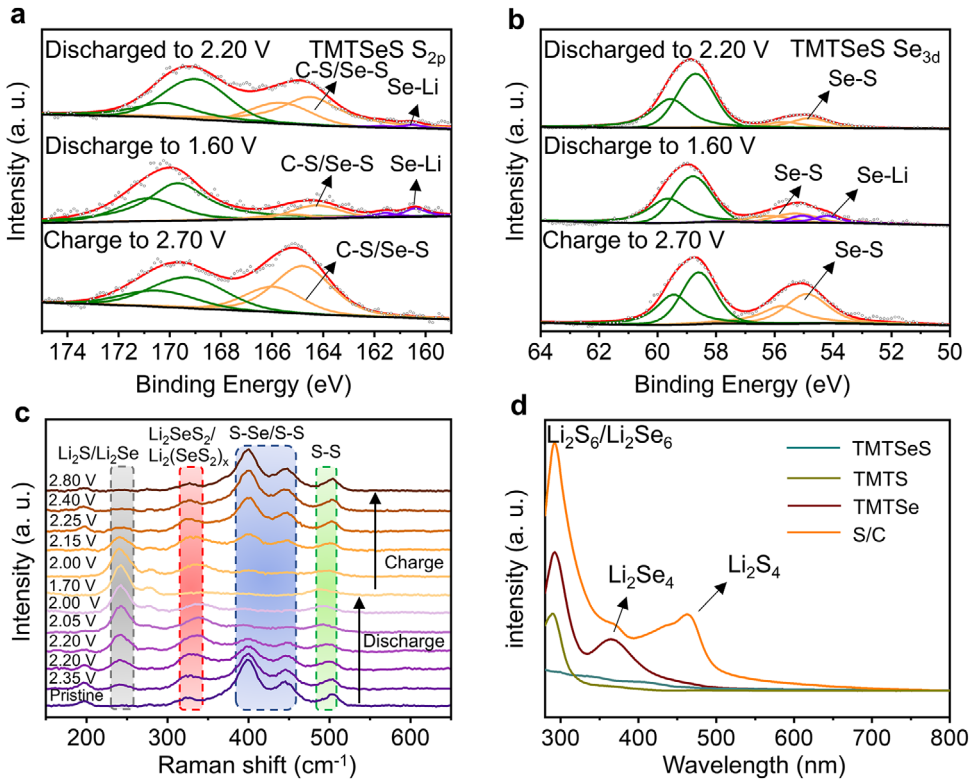

FIGURE 5 | (a, b) XPS spectra at (a) S 2p and (b) Se 3d levels of TMTSeS cathodes at various charging/discharging states. (c) In situ Raman spectra of TMTSeS cathode at various charging/discharging states. (d) UV–vis absorption spectra of DME solutions, respectively soaking with the four types of cathodes at a discharge voltage of 2.25 V.

a reversible conversion of the S—Se—S structural units and further confirming the excellent electrochemical reversibility of the TMTSeS cathode material [43]. Additionally, SEM images and corresponding elemental mappings of C, S, and Se in the TMTSeS cathode at different charge-discharge states are shown in Figure S9. The homogeneous distributions of S and Se in the TMTSeS cathode indicate that the S and Se elements in TMTSeS are well preserved and would not dissolve into the electrolyte during cycling.

Moreover, in situ Raman spectroscopy was employed to validate the charge–discharge mechanism of TMTSeS (Figure 5c). During the discharge phase, the intensities of S—S and S—Se peaks gradually decreased. At a voltage of 2.20 V, a characteristic peak at approximately 360 cm^{-1} corresponding to $Li_2SeS_2/Li_2(SeS_2)_x$ intermediates emerged, indicating the initiation of Li^+ storage in the chain-like sulfur–selenium structures. As discharge continued, this peak first increased in intensity and then gradually disappeared. Upon full discharge to 1.70 V, only peaks corresponding to Li_2S and Li_2Se remained, signifying the completion of lithiation [43–45]. During the charging process, the spectra exhibited the reverse behavior, eventually returning to a state consistent with the pristine TMTSeS cathode. These observations further confirm the reversible charge–discharge behavior of the TMTSeS cathode and are consistent with the mechanism involving the chain-like S—Se structure that provides high conductivity and abundant lithium storage sites. Moreover, this behavior explains the material's ability to suppress the formation of soluble polysulfide and polyselenide intermediates, thereby improving cycling stability.

To assess the structural integrity of TMTSeS after long-term cycling, various cathodes, including TMTSeS, TMTS, TMTSe, and conventional S/C composite, were disassembled from the batteries after 400 cycles and immersed in a dimethoxyethane (DME) solution for UV–vis absorption spectroscopy characterizations (Figure 5d). For the TMTS, TMTSe, and S/C cathodes, the absorption peaks at 300, 360, and 460 nm indicate the presence of Li_2S_6 (or Li_2Se_6) and Li_2S_4 (or Li_2Se_4) [30, 46]. Especially, the S/C composite electrode-soaked DME solution exhibited the strongest absorption peaks at 300 nm and 460 nm, indicating the production of plentiful polysulfides. This intensive polysulfide formation would lead to a severe shuttle effect during cycling, resulting in rapid capacity decay of S/C composite cathode (Figure S10). In sharp contrast, the UV–vis absorption spectrum of TMTSeS electrode-soaked DME solution exhibited no detectable peaks corresponding to polysulfides (Li_2S_6) or polyselenides (Li_2Se_6 or Li_2Se_4), conducive to its sulfur-selenium hybrid molecular chain structure. This result intuitively confirms that the TMTSeS cathode can effectively prevent the shuttle effect, thereby improving the cycle lifespan of lithium-organochalcogenide batteries.

3 | Conclusion

In summary, this study reports the design and synthesis of linearly bonded organoselenide-sulfide hybrid compound cathode material as a transformative candidate to address the critical challenges of chalcogen-based cathodes caused by the low conductivity and the shuttle effect of polychalcogenide anions. The as-prepared TMTSeS compound possesses

chain-like structure with improved conductivity and high chalcogen atom ratios, resulting in greatly boosted electrochemical performances via dual mechanisms involving chemical adsorption and electrochemical conversion. A series of electrochemical tests and spectroscopic analyses verify that this configuration effectively suppresses the shuttle effect during battery cycling while simultaneously enhancing material structural stability. The resulting TMTSeS cathode demonstrates favorable battery performances, achieving a high specific capacity of 816.8 mAh g^{-1} at 1.0 A g^{-1} and an ultra-low capacity decay rate of 0.06% per cycle. These findings highlight the intriguing potential of organoselenide-sulfide hybrid compounds, providing a viable pathway to further advance lithium-organochalcogenide battery technology toward high-specific-energy, low-cost, and eco-friendly applications.

Author Contributions

Z. J. and X. M. conceived the idea of this study. X. M. performed the preparation of materials. X. M. and H. L. performed the FT-IR, Raman and XPS analyses. X. M., Y. W., T. Y., and X. S. performed the electrochemical measurements. X. M., H. L., J. L., Z. W., H. W., J. W., L. Q., and Z. T. contributed to the data analysis. Z. J. and X. M. analyzed the data and wrote the paper. Z. J. revised the manuscript and supervised the project. All authors discussed the results and commented on the manuscript.

Acknowledgements

This work was supported by the National Natural Science Foundation of China (U25A20628, 22561160129, 22479074, 22475096), the Equipment Pre-Research and Ministry of Education Joint Fund (8091B02052407), the Fundamental Research Program Key Project of Jiangsu Province (BK20253008), the Science and Technology Major Project of Jiangsu Province (BG2024013), the Scientific and Technological Achievements Transformation Special Fund of Jiangsu Province (BA2023037), the Academic Degree and Postgraduate Education Reforming Project of Jiangsu Province (JGKT24_C001), the Key Core Technology Open Competition Project of Suzhou City (SYG2024122), the Open Research Fund of Suzhou Laboratory (SZLAB-1308-2024-TS005), the Chenzhou National Sustainable Development Agenda Innovation Demonstration Zone Provincial Special Open Competition Project (2023sfq11, 2025sfq38), and the Fundamental Research Funds for the Central Universities and Nanjing University International Collaboration Initiative (020514380354).

Conflicts of Interest

The authors declare no conflicts of interest.

Data Availability Statement

The data that support the findings of this study are available from the corresponding author upon reasonable request.

References

1. C. Zhao, G. Xu, Z. Yu, et al., "Author Correction: a High-Energy and Long-Cycling Lithium–Sulfur Pouch Cell via a Macroporous Catalytic Cathode with Double-End Binding Sites," *Nature Nanotechnology* 16 (2021): 224–224, https://doi.org/10.1038/s41565-020-00797-w.

2. Z. Wang, Y. Dong, H. Li, et al., "Enhancing Lithium–Sulphur Battery Performance by Strongly Binding the Discharge Products on Amino-Functionalized Reduced Graphene Oxide," *Nature Communications* 5 (2014): 5002, https://doi.org/10.1038/ncomms6002.

3. Y. Liu, S. Liu, G. R. Li, and X. P. Gao, "Strategy of Enhancing the Volumetric Energy Density for Lithium–Sulfur Batteries," *Advanced Materials* 33, no. 8 (2021): 2003955, https://doi.org/10.1002/adma.202003955.

4. Z. Liang, D. Yang, P. Tang, et al., "Atomically Dispersed Fe in a C_2N Based Catalyst as a Sulfur Host for Efficient Lithium–Sulfur Batteries," *Advanced Energy Materials* 11, no. 5 (2021): 2003507, https://doi.org/10.1002/aenm.202003507.

5. B. Jin, L. Yang, J. Zhang, et al., "Bioinspired Binders Actively Controlling Ion Migration and Accommodating Volume Change in High Sulfur Loading Lithium–Sulfur Batteries," *Advanced Energy Materials* 9, no. 48 (2019): 1902938, https://doi.org/10.1002/aenm.201902938.

6. L. Wang, X. Yin, C. Jin, C. Lai, G. Qu, and G. Zheng, "Cathode-Supported-Electrolyte Configuration for High-Performance all-Solid-State Lithium-Sulfur Batteries," *ACS Applied Materials & Interfaces* 3, no. 12 (2020): 11540–11547, https://doi.org/10.1021/acsaem.0c02347.

7. Y. Ren, B. Wang, H. Liu, et al., "CoP Nanocages Intercalated MXene Nanosheets as a Bifunctional Mediator for Suppressing Polysulfide Shuttling and Dendritic Growth in Lithium-Sulfur Batteries," *Chemical Engineering Journal* 450, no. 3 (2022): 138046, https://doi.org/10.1016/j.cej.2022.138046.

8. Y. Xiao, Y. Xiang, S. Guo, et al., "An Ultralight Electroconductive Metal-Organic Framework Membrane for Multistep Catalytic Conversion and Molecular Sieving in Lithium-Sulfur Batteries," *Energy Storage Materials* 51 (2022): 882–889, https://doi.org/10.1016/j.ensm.2022.07.018.

9. A. Eftekhari, "High-Energy Aqueous Lithium Batteries," *Advanced Energy Materials* 8, no. 24 (2018): 81801156, https://doi.org/10.1002/aenm.201801156.

10. F. Wan, L. Fang, X. Zhang, C. A. Wolden, and Y. Yang, "Lithium Sulfide Nanocrystals as Cathode Materials for Advanced Batteries," *Journal of Energy Chemistry* 63 (2021): 138–169, https://doi.org/10.1016/j.jechem.2021.09.028.

11. Y. V. Mikhaylik and J. R. Akridge, "Polysulfide Shuttle Study in the Li/S Battery System," *Journal of The Electrochemical Society* 151 (2004): A1969–A1976, https://doi.org/10.1149/1.1806394.

12. G. Li, S. Wang, Y. Zhang, M. Li, Z. Chen, and J. Lu, "Revisiting the Role of Polysulfides in Lithium–Sulfur Batteries," *Advanced Materials* 30, no. 22 (2018): 1705590, https://doi.org/10.1002/adma.201705590.

13. A. Manthiram, Y. Fu, and Y. S. Su, "Challenges and Prospects of Lithium–Sulfur Batteries," *Accounts of Chemical Research* 46, no. 5 (2013): 1125–1134, https://doi.org/10.1021/ar300179v.

14. J. Balach, T. Jaumann, M. Klose, S. Oswald, J. Eckert, and L. Giebeler, "Functional Mesoporous Carbon-Coated Separator for Long-Life, High-Energy Lithium-Sulfur Batteries," *Advanced Functional Materials* 25, no. 33 (2015): 5285–5291, https://doi.org/10.1002/adfm.201502251.

15. B. Moorthy, S. Kwon, J.-H. Kim, P. Ragupathy, H. M. Lee, and D. K. Kim, "Tin Sulfide Modified Separator as an Efficient Polysulfide Trapper for Stable Cycling Performance in Li–S Batteries," *Nanoscale Horizons* 4, no. 1 (2019): 214–222, https://doi.org/10.1039/c8nh00172c.

16. J. Xu, Q. Zhang, X. Liang, J. Yan, J. Liu, and Y. Wu, "A Multifunctional Separator Based on Scandium Oxide Nanocrystal Decorated Carbon Nanotubes for High Performance Lithium–Sulfur Batteries," *Nanoscale* 12, no. 12 (2020): 6832–6843, https://doi.org/10.1039/d0nr00160k.

17. Y. Jiang, H. Arshad, H. Li, S. Liu, G. Li, and X. Gao, "Crystalline Multi-Metallic Compounds as Host Materials in Cathode for Lithium-Sulfur Batteries," *Small* 17, no. 22 (2021): 2005332, https://doi.org/10.1002/smll.202005332.

18. L. Feng, P. Yu, X. Fu, et al., "Regulating Polysulfide Diffusion and Deposition via Rational Design of Core–Shell Active Materials in Li–S Batteries," *ACS Nano* 16, no. 5 (2022): 7982–7992, https://doi.org/10.1021/acsnano.2c00882.

19. Y. Tsao, Z. Chen, S. Rondeau-Gagné, et al., "Enhanced Cycling Stability of Sulfur Electrodes through Effective Binding of Pyridine-

Functionalized Polymer," *ACS Energy Letters* 2, no. 10 (2017): 2454–2462, https://doi.org/10.1021/acsenergylett.7b00772.

20. Z. Ma, Y. Liu, J. Gautam, et al., "Embedding Cobalt Atom Clusters in CNT-Wired MoS_2 Tube-In-Tube Nanostructures with Enhanced Sulfur Immobilization and Catalyzation for Li-S Batteries," *Small* 17, no. 39 (2021): 2012710, https://doi.org/10.1002/smll.202102710.

21. P. Liu, W. Yang, F. Xiao, Y. Qi, S. Jamil, and M. Xu, "Efficient Anchoring of Polysulfides Based on Self-Assembled $Ti_3C_2T_x$ Nanosheet-Connected Hollow $Co(OH)_2$ Nanotubes for Lithium–Sulfur Batteries," *ACS Applied Materials & Interfaces* 13, no. 48 (2021): 57285–57293.

22. J. Zhang, H. Hu, Z. Li, and X. Lou, "Double-Shelled Nanocages with Cobalt Hydroxide Inner Shell and Layered Double Hydroxides Outer Shell as High-Efficiency Polysulfide Mediator for Lithium–Sulfur Batteries," *Angewandte Chemie International Edition* 55, no. 12 (2016): 3982–3986, https://doi.org/10.1002/ange.201511632.

23. Z. Li, J. Zhang, and X. Lou, "Hollow Carbon Nanofibers Filled with MnO_2 Nanosheets as Efficient Sulfur Hosts for Lithium–Sulfur Batteries," *Angewandte Chemie International Edition* 54, no. 44 (2015): 12886–12890, https://doi.org/10.1002/ange.201506972.

24. Y. Liu, K. Xiao, S. Yang, et al., "Organic Electrolyte Additive: Dual Functions toward Fast Sulfur Conversion and Stable Li Deposition for Advanced Li–S Batteries," *Small* 20, no. 30 (2024): 2309890, https://doi.org/10.1002/smll.202309890.

25. Z. Zhao, B. Desalegn, H. Joe, et al., "*In-situ* Construction of an Alloy Hybrid Interface and Ultrathin ZnS Nanosheets Catalyst for Polysulfide by Trifunctional ZnI_2 Electrolyte Additive for Li-S Batteries," *Energy Storage Materials* 73 (2024): 103862, https://doi.org/10.1016/j.ensm.2024.103862.

26. J. Lian, W. Guo, and Y. Fu, "Isomeric Organodithiol Additives for Improving Interfacial Chemistry in Rechargeable Li–S Batteries," *Journal of the American Chemical Society* 143, no. 29 (2021): 11063–11071, https://doi.org/10.1021/jacs.1c04222.

27. X. Zhang, T. Yu, S. Yang, et al., "Organosulfur Cathodes in Lithium Metal Batteries: Bridging the Gap between Fundamentals and Practical Applications," *Advanced Functional Materials* 34 (2024): 2405122, https://doi.org/10.1002/adfm.202405122.

28. H. Li, H. Yang, and X. Ai, "Routes to Electrochemically Stable Sulfur Cathodes for Practical Li–S Batteries," *Advanced Materials* 37 (2023): 2305038, https://doi.org/10.1002/adma.202305038.

29. T. Zhang, F. Hu, W. Shao, et al., "Sulfur-Rich Polymers Based Cathode with Epoxy/Ally Dual-Sulfur-Fixing Mechanism for High Stability Lithium–Sulfur Battery," *ACS Nano* 15, no. 9 (2021): 15027–15038, https://doi.org/10.1021/acsnano.1c05330.

30. X. Ma, H. Li, J. Liang, et al., "Heterocycle-Bridged Short Sulfur-Chain Polymers for Polysulfide-Suppressing Cathodes in Lithium-Organosulfide Batteries," *Advanced Energy Materials* 16 (2026): 06388, https://doi.org/10.1002/aenm.202506388.

31. J. Zhang, M. Wu, Z. Zhang, N. Li, C. Tian, and W. Xue, "Sparingly Solvating Electrolyte with Hofmeister Selectivity for Practical Long-Lived Li-Se Batteries," *Angewandte Chemie International Edition* 64 (2025): 11223, https://doi.org/10.1002/anie.202511223.

32. Z. Zhang, H. Peng, M. Zhao, and J. Huang, "Heterogeneous/Homogeneous Mediators for High-Energy-Density Lithium-Sulfur Batteries: Progress and Prospects," *Advanced Functional Materials* 28, no. 38 (2018): 1707536, https://doi.org/10.1002/adfm.201707536.

33. J. Liu, M. Wang, N. Xu, T. Qian, and C. Yan, "Progress and Perspective of Organosulfur Polymers as Cathode Materials for Advanced Lithium-Sulfur Batteries," *Energy Storage Materials* 15 (2018): 53–64, https://doi.org/10.1016/j.ensm.2018.03.017.

34. F. Wang, C. Yang, Y. Wang, et al., "Heterostructure: Application of Absorption-Catalytic Center in Lithium-Sulfur Batteries," *Rare Metals* 43, no. 4 (2024): 1461–1487, https://doi.org/10.1007/s12598-023-02486-8.

35. J. Zhou, C. Shu, Q. Zhang, W. Tang, and Y. Wu, "Tandemly Promoting the Sulfur Redox Kinetics through Low Concentration Mixed Organodiselenide and Organoditelluride in Ah-Level High-Energy-Density Li-S Batteries," *Science China Materials* 68 (2024): 207–216, https://doi.org/10.1007/s40843-024-3173-9.

36. J. H. Kim, M. Kim, S.-J. Kim, et al., "Understanding the Electrochemical Processes of SeS_2 Positive Electrodes for Developing High-Performance Non-Aqueous Lithium Sulfur Batteries," *Nature Communications* 15 (2024): 7669, https://doi.org/10.1038/s41467-024-51647-5.

37. M. Preefer, B. Oschmann, C. Hawker, R. Seshadri, and F. Wudl, "High Sulfur Content Material with Stable Cycling in Lithium-Sulfur Batteries," *Angewandte Chemie International Edition* 56, no. 47 (2017): 15118–15122, https://doi.org/10.1002/ange.201708746.

38. H. Kim, J. Lee, H. Ahn, O. Kim, and M. Park, "Synthesis of Three-Dimensionally Interconnected Sulfur-Rich Polymers for Cathode Materials of High-Rate Lithium–Sulfur Batteries," *Nature Communications* 6 (2015): 7278, https://doi.org/10.1038/ncomms8278.

39. N. Feng, K. Xiang, L. Xiao, et al., "Se/CNTs Microspheres as Improved Performance for Cathodes in Li-Se Batteries," *Journal of Alloys and Compounds* 786 (2019): 537–543, https://doi.org/10.1016/j.jallcom.2019.01.348.

40. J. Xu, F. Yu, J. Hua, et al., "Donor Dominated Triazine-Based Microporous Polymer as a Polysulfide Immobilizer and Catalyst for High-Performance Lithium-Sulfur Batteries," *Chemical Engineering Journal* 392 (2020): 123694, https://doi.org/10.1016/j.cej.2019.123694.

41. R. Sun, Y. Bai, M. Luo, Z. Wang, W. Sun, and K. Sun, "Enhancing Polysulfide Confinement and Electrochemical Kinetics by Amorphous Cobalt Phosphide for Highly Efficient Lithium–Sulfur Batteries," *ACS Nano* 15, no. 1 (2021): 739–750, https://doi.org/10.1021/acsnano.0c07038.

42. Z. Wang, J. An, K. Xie, et al., "Situ Organoselenization for Ultrastable Li−Se Batteries," *Advanced Materials* 38 (2026): 23054, https://doi.org/10.1002/adma.202523054.

43. V. Pham, J. Boscoboinik, D. Stacchiola, et al., "Selenium-Sulfur (SeS) Fast Charging Cathode for Sodium and Lithium Metal Batteries," *Energy Storage Materials* 20 (2019): 71–79, https://doi.org/10.1016/j.ensm.2019.04.021.

44. L. Ma, Y. Wang, Z. Wang, et al., "Wide-Temperature Operation of Lithium–Sulfur Batteries Enabled by Multi-Branched Vanadium Nitride Electrocatalyst," *ACS Nano* 17, no. 12 (2023): 11527–11536, https://doi.org/10.1021/acsnano.3c01469.

45. X. Lv, Z. Qian, X. Zhang, et al., "Enhancement of Overall Kinetics by Se−Br Chemistry in Rechargeable Li−S Batteries," *Angewandte Chemie International Edition* 63 (2024): 202405880, https://doi.org/10.1002/anie.202405880.

46. A. Tao, K. Zhang, X. Ma, et al., "Building Lithium-Polycarbonsulfide Batteries with High Energy Density and Long Cycling Life," *ACS Energy Letters* 8 (2023): 79–89, https://doi.org/10.1021/acsenergylett.2c02107.

Supporting Information

Additional supporting information can be found online in the Supporting Information section.

Supporting File: aenm71215-sup-0001-SuppMat.docx.